Solar Phys (2014) 289:2433–2457
DOI 10.1007/s11207-014-0474-1

Accurate Determination of the TOA Solar Spectral NIR Irradiance Using a Primary Standard Source and the Bouguer–Langley Technique

D. Bolsée · N. Pereira · W. Decuyper · D. Gillotay · H. Yu · P. Sperfeld · S. Pape · E. Cuevas · A. Redondas · Y. Hernandéz · M. Weber

Received: 30 April 2013 / Accepted: 2 January 2014 / Published online: 16 January 2014
© Springer Science+Business Media Dordrecht 2014

Abstract We describe an instrument dedicated to measuring the top of atmosphere (TOA) solar spectral irradiance (SSI) in the near-infrared (NIR) between 600 nm and 2300 nm at a resolution of 10 nm. Ground-based measurements are performed through atmospheric NIR windows and the TOA SSI values are extrapolated using the Bouguer–Langley technique. The interest in this spectral range arises because it plays a main role in the Earth's radiative budget and also because it is employed to validate models used in solar physics. Moreover, some differences were observed between recent ground-based and space-based instruments that take measurements in the NIR and the reference SOLSPEC(ATLAS3) spectrum. In the 1.6 μm region, the deviations vary from 6 % to 10 %. Our measuring system named IRSPERAD has been designed by Bentham (UK) and has been radiometrically characterized and absolutely calibrated against a blackbody at the Belgian Institute for Space Aeronomy and at the Physikalisch-Technische Bundesanstalt (Germany), respectively. A four-month measurement campaign was carried out at the Izaña Atmospheric Observatory (Canary Islands, 2367 m a.s.l.). A set of top-quality solar measurements was processed to obtain the TOA SSI in the NIR windows. We obtained an average standard uncertainty of 1 % for 0.8 μm $< \lambda <$ 2.3 μm. At 1.6 μm, corresponding to the minimum opacity of the solar photosphere, we obtained an irradiance of 234.31 ± 1.29 mWm^{-2} nm^{-1}. Between 1.6 μm

Electronic supplementary material The online version of this article (doi:10.1007/s11207-014-0474-1) contains supplementary material, which is available to authorized users.

D. Bolsée (✉) · N. Pereira · W. Decuyper · D. Gillotay · H. Yu
BIRA-IASB, 3 Avenue Circulaire, 1180 Brussels, Belgium
e-mail: david.bolsee@aeronomie.be

P. Sperfeld · S. Pape
Physikalisch-Technische Bundesanstalt, Braunschweig, Germany

E. Cuevas · A. Redondas · Y. Hernandéz
Izaña Atmospheric Research Center (AEMET), Tenerife, Spain

M. Weber
Institut für Umweltphysik, Universität Bremen, Bremen, Germany

and 2.3 μm, our measurements show a disagreement varying from 6 % to 8 % relative to ATLAS3, which is not explained by the declared standard uncertainties of the two experiments.

Keywords Ground-based · Near-infrared · Solar spectral irradiance · Top of atmosphere

1. Introduction

The visible and infrared continuum radiation of the Sun are emitted by the solar photosphere, which is a 300 km thick layer corresponding to the top of the Sun's convective zone. The photosphere exhibits a negative temperature gradient and its spectral irradiance distribution is approximated by the emission of a blackbody at 5870 K. The integrated radiation between 700 nm and 2400 nm accounts for approximately half of the total solar irradiance (TSI). From standard solar physics and observations it is well established that for increasing wavelengths (from 0.8 μm up to 1.6 μm), radiation is progressively produced in regions deeper in the photosphere (Fontenla *et al.*, 2004). The minimum absorption coefficient and the minimum opacity values are reached at 1.6 μm, corresponding to the maximum brightness temperature value. Above this wavelength, radiation originates from progressively higher layers.

Near-infrared (NIR) solar irradiance plays an important role in both the Earth's radiative budget (atmospheric absorption by H_2O, CO_2, O_3, and O_2 and the absorption by the upper layer of ocean waters) and in the modelling of climatology and photochemistry of Earth's atmosphere (Harder *et al.*, 2005). Therefore the exo-atmospheric NIR solar irradiance has to be determined with a high accuracy, which could also benefit the validation of models used in solar physics.

The performance of a given electromagnetic radiation detection systems is ultimately limited by noise. In the particular case of infrared technology, semiconductor materials are widely used, both in the radiation detectors and in the amplification circuits. Semiconductors are known to be intrinsic sources of thermal noise that add to the unavoidable background photon noise. The signal levels arising from the detection of low-energy NIR photons might not be sufficient to exceed such noise. Therefore, cooled and sensitive phase detection systems are a solution to overcome low signal levels (Kruse, McGlauchlin, and McQuistan, 1962). Conducting top of atmosphere (TOA) measurements from space implies, among other difficulties, having scant control over absolute radiometric scales. Although ground-based measurements do not present this disadvantage, strong or even complete extinction by molecular absorption in Earth's atmosphere exists in several spectral regions. Therefore only a few narrow spectral ranges (atmospheric windows) are available. In addition, Rayleigh scattering and aerosol extinction is present for the whole spectra. These factors contribute to the relative paucity of NIR exo-atmospheric measurements.

The first measurement from a satellite was made in 1992 – 1993 by the SOSP version of SOLSPEC on EURECA (Thuillier *et al.*, 1981), a space-qualified spectroradiometer absolutely calibrated against a blackbody as a primary standard source (Mandel *et al.*, 1998). This led to the publication of the reference ATLAS3 spectrum from 200 nm to 2400 nm (Thuillier *et al.*, 2003) for which the announced standard uncertainty was around 3 %. This spectrum was used to validate the semi-empirical models of solar atmosphere in the NIR (Fontenla *et al.*, 2006). Before ATLAS3, as reviewed in detail in Thuillier *et al.* (2003), only the measurements at high altitude (Neckel and Labs, 1984) or from an airplane were available (Arvesen, Griffin, and Pearson, 1969).

The contribution from Arvesen, Griffin, and Pearson (1969) to the determination of TOA SSI was of great importance: it benefited from well-characterized instrumentation and the quasi-transparency of the atmosphere encountered at 12 km in some NIR wavelength ranges. A 1000 W quartz-halogen lamp was used as an in-flight calibration device.

In the past decade, the TOA solar irradiance was provided by three new space instruments: the *Solar Irradiance Monitor* (SIM), a prism spectrometer on board the *Solar Radiation and Climate Experiment* (SORCE; Harder *et al.*, 2000), providing daily measurements up to 2.4 μm since 2003; the *Scanning Imaging Absorption Spectrometer for Atmospheric Chartography* (SCIAMACHY; Noël *et al.*, 1998), a remote-sensing spectrometer with NIR channels and capabilities up to 2.4 μm (2002 – 2012); since 2008, the *SOLar SPECtrum* (SOLAR/SOLSPEC; Thuillier *et al.*, 2009) on board the International Space Station (ISS), containing an improved IR channel at electronic and optic levels, and a highly accurate absolute calibration against the Physikalisch-Technische Bundesanstalt (PTB; Braunschweig, Germany) blackbody standard of irradiance (Sperfeld *et al.*, 1995; Sapritsky *et al.*, 1997).

More recently, in 2013, ground-based TOA SSI measurements were retrieved by the Langley-plot method using a high-resolution Fourier Spectrometer, absolutely calibrated against the National Physical Laboratory's (NPL, Teddington, UK) blackbody. The published Continuum Absorption at Visible and Infrared Wavelengths and its Atmospheric Relevance Extraterrestrial Solar Spectrum (CAVIAR ESS) covers the spectral range from 1 μm to 2.5 μm (Menang *et al.*, 2013).

While comparing SIM to the reference ATLAS3, a systematic trend not well understood was observed above 1 μm, with SIM being systematically lower. The SIM-to-ATLAS3 bias correction reached a value of -8 % near 1.5 μm, remaining constant for longer wavelengths (Harder *et al.*, 2010). For SCIAMACHY, hardware constraints limited the available data to 1.7 μm (Pagaran, Weber, and Burrows, 2009). Above 1 μm, SCIAMACHY diverges progressively from ATLAS3, reaching a maximum deviation in the region of 1.6 μm (Pagaran *et al.*, 2011). The NIR SOLAR/SOLSPEC (Thuillier *et al.*, 2013) shows a non-negligible discrepancy with ATLAS3 in the wavelength range of 1.2 μm to 2.2 μm. This discrepancy is of 8 % at 1.6 μm, reaching a maximum of 12 % at 1.8 μm. Future space measurements on the NIR range will be provided by an improved and calibrated version of SIM on the *Total Solar Irradiance Sensor* (TSIS; Cahalan, Pilewskie, and Woods, 2012).

CAVIAR ESS measurements showed an average deviation of 8.3 % to ATLAS3 in the 1.4 μm to 2.4 μm wavelength range. The absence of overlapping of the error bars (at a 95 % confidence interval) does not allow for an inter-validation between the two experiments. However, the deviation in this wavelength range is consistent with those observed in recent experiments (namely SCIAMACHY and SOLAR/SOLSPEC), as explained above.

Given this review, a new ground-based campaign is of great importance, with the objective being the accurate measurement of absolute irradiance values for several atmospheric windows in the NIR. The accuracy and quality of these measurements is expected to be sufficient to bear a significant contribution to resolve the discrepancies in the NIR SSI observed from space. Because this ground-based campaign is conducted by the same team that renewed the hardware of the infrared channel of SOLAR/SOLSPEC, the new set of ground measurements is realized with similar instrumental conditions to those of SOLAR/SOLSPEC, namely the same detection technique (phase-sensitive detection) and identical spectral ranges and bandwidth. Furthermore, a high-quality absolute radiometric calibration is performed. The primary standard of spectral irradiance reference used for SOLAR/SOLSPEC, the blackbody BB3200pg of PTB, is used for absolute calibration. These measurements have to be conducted at high altitude, at a site with stable meteorological conditions with a high level of Sun exposure and prevalence of clear-sky conditions. The

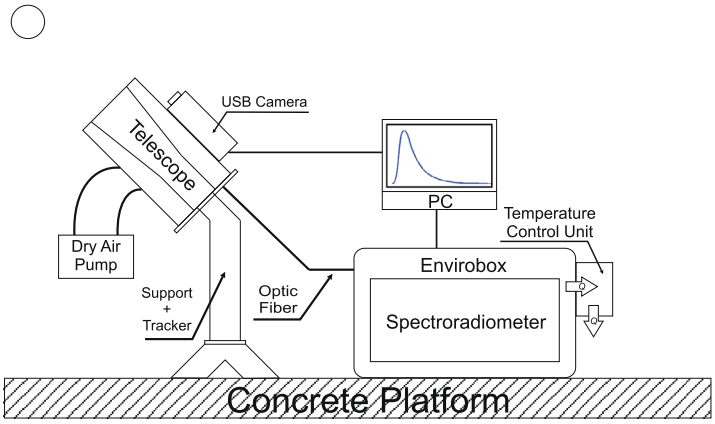

Figure 1 The IRSPERAD experimental setup deployed at Izaña Atmospheric Observatory (IZO).

Izaña Atmospheric Observatory (IZO) fulfils all these requirements (Puentedura *et al.*, 2012; García *et al.*, 2013), and moreover, it offers excellent logistic and personnel support conditions to perform a solar irradiance measurement campaign.

2. Methodology

2.1. Instrumentation

The complete measurement system InfraRed SPEctroRADiometer (IRSPERAD) is composed of a spectroradiometer and associated electronics, enclosed in a temperature-stabilized waterproof container (envirobox). An optic fibre and a telescope form the ensemble of the entrance optics, which are attached to a Sun-tracker device. A schematic illustration of the fully experimental setup is shown in Figure 1.

The spectroradiometer used is a DMc-150-IR model from the Bentham company, which is composed of a double Czerny–Turner monochromator in an additive configuration. Radiation is detected by a PbS cell. Table 1 summarizes the spectroradiometer characteristics, compared with those of SOLAR/SOLSPEC.

The Sun-tracking device is an STR-21 model from the company EKO. The tracker is equipped with a four-quadrant silicon-photodiode detector. The balance of currents measured by each of the photodiodes prompts the motion of the tracker, with an accuracy of $\pm 0.1°$, so that it becomes aligned with the solar disk. When the Sun is visible, the tracker works in Sun-tracking mode, switching to calculation mode otherwise. In this mode, the Sun's position is calculated by means of an internal CPU. The switch between modes is determined by a solar irradiance threshold value calculated at the corresponding air mass value.

A custom sunlight-collecting telescope was designed following the standards for direct irradiance measurements according to the Commission for Instruments and Methods of Observation (CIMO; 2008). The values for the slope and opening half angles, as defined in Figure 2, are 1.4° and 3.6°, producing a 7.2° field of view (FOV). These values were obtained by means of three concentric pinholes and a quartz diffuser as seen in Figure 3. From

Table 1 Comparison of the main characteristics of the infrared spectroradiometers used in IRSPERAD and in SOLAR/SOLSPEC on board ISS.

	IRSPERAD	SOLAR/SOLSPEC
Detector		
Type	PbS cell	PbS cell
Peak sensitivity (μm)	2.7	2.5
Working temperature (°C)	− 10	− 20
Chopper frequency (Hz)	225	512
Monochromators		
Configuration	Double Czerny–Turner	Double Czerny–Turner
Grating type	Plane grating	Concave grating
Groove density (mm^{-1})	600	353.83
Entrance optics		
Material	Primusil® OQ[a]	Double Suprasil®[b]
Thickness (mm)	1	1
Slit width (mm)		
entrance/middle/exit	1.85/1.85/1.85	0.2/0.4/0.4
Total focal length (mm)	300	229.77
Spectral range (nm)	600 – 2400	650 – 3080
Nominal bandwidth (nm)	10	8[c]
	700	490
High-order filters (nm)	1250	875
	2000	1600

[a]SGIL GmbH.

[b]Heraeus GmbH.

[c]the bandwidth, which is wavelength dependent, is given at the middle of the spectral range.

the diffuser, sunlight is injected into a 6 m long optic fibre and guided towards the spectrometer. The fibre is a bundle composed of 100 μm mono-fibres. The bundle has a 2 mm diameter entrance and a 1×3.1 mm^2 output slit.

The high-order filter wheel is located inside of the first monochromator's entrance port, after the entrance slit.

2.2. Radiometric Characterization

The spectrometer has been fully characterized in the Belgian Institute for Space Aeronomy (BIRA-IASB) laboratory. Studies have been conducted to determine the signal-to-noise ratio (SNR), the accuracy and reproducibility of the wavelength scale of the instrument, and the influence of the temperature on the response of the detector.

2.2.1. Signal-to-Noise Ratio

The SNR of the detector was determined in the laboratory. The SNR was calculated for ten different signal levels, spanning a minimum of three decades of the dynamical range, from 2.5×10^{-2} V to 3.2 V. A stable tungsten lamp was used as light source for the measurements that consisted of accumulating a large sampling for each signal level, measured in volt (V).

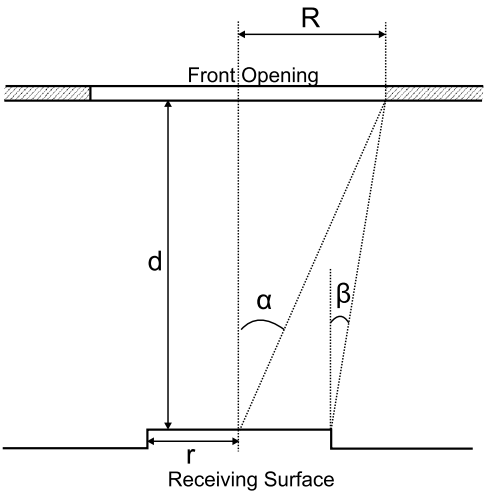

Figure 2 Geometric scheme of the telescope (not to scale). R and r are the radii of the telescope's window and receiving surface, respectively. They are related to the slope and opening half angles, α and β, by the expressions $\alpha = \arctan(\frac{R}{d})$ and $\beta = \arctan(\frac{R-r}{d})$.

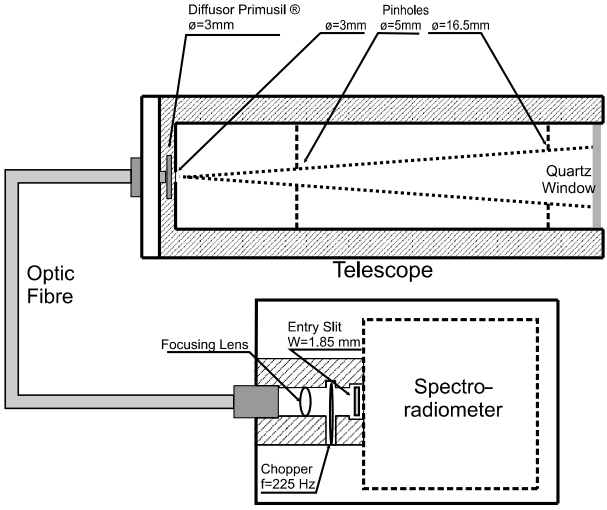

Figure 3 Schematics of the entrance optics of IRSPERAD (not to scale). It includes the Sun collecting device (telescope), the optic fibre, the focusing optics, and the chopper.

The noise inherent to each signal level was defined as the standard deviation of the given sampling. Figure 4 shows the SNR curve as a function of the measured signal.

2.2.2. Wavelength Scale and Spectral Bandwidth

Two wavelength samplings were defined. The first one was conceived for nominal acquisitions, from 600 nm to 2300 nm by increments of 5 nm. The second one (custom sampling) was defined to avoid the broad bands of H_2O molecular absorptions around 0.94 µm, 1.12 µm, 1.37 µm, and 1.87 µm, where partial or complete extinction can occur. Both wavelength samplings were used during the calibrations. The solar measurements were mainly performed using the custom sampling. The signature of water vapour absorption was modelled from the HITRAN 2008 cross-sections database. For an optical path of 1.25 m, measured at the laboratory, we found an extinction of 17 % at 1.87 µm. The steep signal drops

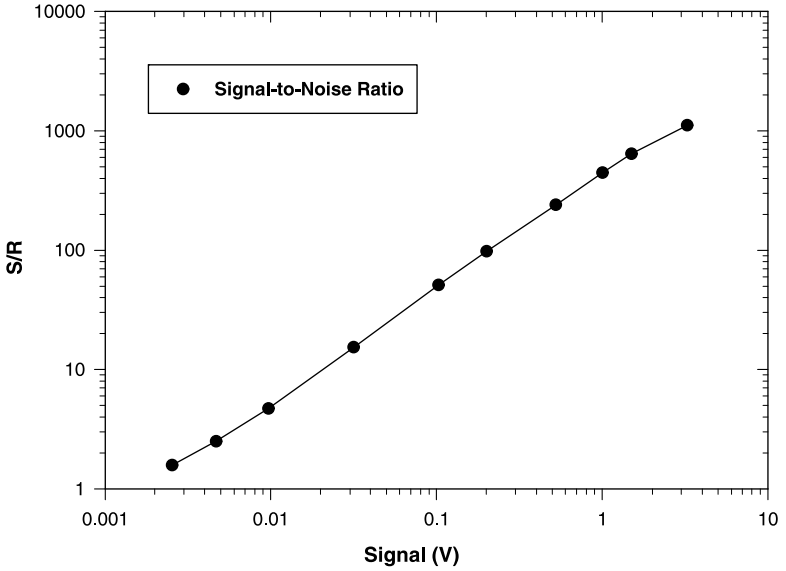

Figure 4 SNR curve of the detector. The noise was calculated as the standard deviation of a given signal level, σ(signal), for a large number of measurements. The quantity SNR is defined as $\mathrm{SNR} = \frac{\overline{\mathrm{signal}}}{\sigma(\mathrm{signal})}$.

in these bands induce several gain changes in the pre-amplifier, each gain change requiring a non-negligible stabilization time. By skipping the measurements of these bands, the acquisition time for the solar spectra was reduced.

The wavelength scale of the spectrometer was fully characterized using distinct wavelength control methods. On one hand, the measurement of several emission lines of five He–Ne lasers at different wavelengths in combination with xenon, argon, and krypton arc lamps, permitted us to determine the accuracy in the absolute wavelength scale. On the other hand, the monitoring of the position of water vapour absorption structures (for the laboratory measurements) and a set of CO_2, O_3, and O_2 atmospheric absorption bands in the NIR solar spectrum allowed us to determine relative wavelength shifts that might have occurred during the campaign and the transport of the equipment.

These methods permitted us to establish fine corrections in the wavelength scale. The maximum error introduced by these corrections is 0.2 nm. From the measurement of a second-order emission peak of the He–Ne laser of 632.8 nm, the full width at half maximum (FWHM) of 10.43 nm is the effective bandwidth of the detector.

2.2.3. Thermal Study

As described in Section 2.1, the envirobox is equipped with an external temperature controller unit that stabilizes the internal temperature at 24.7 °C. For outdoor measurements, continuous sun-exposure can affect the performances of the thermal regulation. A laboratory thermal study was carried out before the campaign. The change of the detector response as a function of the temperature inside the envirobox was determined. The results are summarized in Table 2 and show a small but spectrally dependent trend in the detector's response under thermal stress. Additionally, we confirmed the stability of the wavelength scale under the same thermal stress.

Table 2 Temperature sensitivity coefficient of the PbS cell (% per °C) as a function of wavelength.

λ [nm]	800	850	1000	1070	1240	1550	1620	1690	2120	2220
α_T [%]	−0.136	−0.137	−0.134	−0.133	−0.123	−0.107	−0.101	−0.095	−0.095	−0.030

2.3. Absolute and Relative Calibrations

2.3.1. Absolute Calibration

The absolute radiometric calibration of the spectrometer was performed using the blackbody radiator BB3200pg of the PTB. It was manufactured by the All-Russian Institute for Optophysical Measurements (VNIIOFI, Moscow) and optimized by the PTB. The blackbody provides very stable fundamental radiometric units by using Planck's law and is the national primary standard for realization and dissemination of spectral irradiance (Sperfeld *et al.*, 1998a, 2000, 2010). The BB3200pg has been described and characterized in detail in Sapritsky *et al.* (1997) and Sperfeld *et al.* (1998a, 2000).

The cavity with a length of 200 mm and inner diameter of 37 mm consists of a stack of pressed pyrographite rings heated by a constant electrical current. The precise blackbody aperture diameter is close to 12 mm. The temperature of the cavity was radiometrically determined by using four filter radiometers that are absolutely calibrated against a cryogenic primary detector standard (Friedrich, Fischer, and Strock, 1995; Werner *et al.*, 2000; Taubert *et al.*, 2003). The temperature was numerically obtained by iteratively solving each integral of the blackbody irradiance weighted by the spectral response of a selected radiometer. The standard measurement uncertainty for the blackbody temperature is 0.44 K and the drift was lower than 0.5 $\mathrm{K\,h^{-1}}$ during all measurements. The spectral irradiance, $E_{\mathrm{BB}}(\lambda)$, produced by the blackbody, is calculated using Planck's law

$$E_{\mathrm{BB}}(\lambda) = \varepsilon_{\mathrm{BB}} \frac{A_{\mathrm{BB}}}{d_{\mathrm{BB}}^2} \frac{c_1}{n_\lambda^2 . \lambda^5} \frac{1}{\exp(\frac{c_2}{n_\lambda . \lambda . T_{\mathrm{BB}}}) - 1}, \tag{1}$$

where

- $\varepsilon_{\mathrm{BB}} = 0.99988 \pm 0.0001$ is the effective emissivity of BB3200pg,
- $A_{\mathrm{BB}} = 111.388 \pm 0.04$ mm^2 is the aperture size of the blackbody,
- $d_{\mathrm{BB}} = 1384.05 \pm 0.05$ mm is the distance to the entry optics,
- $n = 1.00029$ is the refractive index of air,
- $c_1 = \frac{2hc^2}{\pi} = 3.74177153(17) \times 10^{-16}$ Wm^2 is the first radiation constant,
- $c_2 = \frac{hc}{k} = 0.014387770(13)$ mK is the second radiation constant as recommended in Mohr and Taylor (2005, p. 69).

For IRSPERAD, we used the exact same distance, d_{BB}, between the blackbody aperture and the instrument's entrance optics as for the SOLAR/SOLSPEC calibration (Thuillier *et al.*, 2009). In this way, the blackbody aperture was seen by IRSPERAD under a full angle of 0.493°, similar to the angular size of the solar disk ($\approx$0.5 %). The absolute calibration took place in early May 2011, three weeks before the start of the Izaña campaign. During the three hours of signal accumulation, the blackbody irradiance was very stable. The mean cavity temperature was 2890 K with a drift of less than 0.1 $\mathrm{K\,h^{-1}}$. Dry air was flushed inside the telescope and the window cleaned before the calibrations. The absolute response R was

calculated as the ratio between the spectral irradiance E_{BB} disseminated by the blackbody and the signal S_{BB} recorded by IRSPERAD

$$R = \frac{E_{BB}}{S_{BB}}, \tag{2}$$

where S_{BB} and R are expressed in V and $\mathrm{mWm^{-2}\,nm^{-1}}$, respectively.

2.3.2. *Inverse Square Law*

Spectroradiometers absolutely calibrated with a reference standard source at a fixed distance, dedicated to spectral irradiance measurements, must verify the inverse square law, which states that a relative factor change for the signal between initial and final positions (d_1, d_2), in front of a point source, must be equal to $(d_1/d_2)^2$. An experimental setup was used to move the telescope along the optical axis of the blackbody. The inverse square law was verified for a central region of the NIR spectra for several intermediate distances to the point source, ranging from 410 mm to 1310 mm. This demonstrated that the entrance optics of IRSPERAD is well designed for spectral irradiance measurements.

2.3.3. *Relative Calibration*

The IRSPERAD system used a set of four FEL-type 1000 W NIST lamps to maintain the internal absolute calibration: between measurements at PTB and at both the beginning and the end of the Izaña campaign. The NIST lamps labelled F417, F545, F546, and F547 were used in a relative measuring mode, without the need of their NIST certificates. They were powered at a DC current of 8.2 A, stabilized at 10^{-5} by the means of an HP 6030A power supply. The precision 0.1 Ω standard shunt resistor (model 1682 from Tinsley, UK) was used to certify the 8.2 A setting. Before use, each lamp was carefully aligned on the optical axis of IRSPERAD at a distance of 50 cm from the internal diffuser of the entrance optics using a precision jig and a laser. The lamp holder designed by NIST allowed a reproducible repositioning of the lamp. After 20 min of lamp stabilization, the scans were repeated and accumulated during 1 h. The first relative calibration with the lamps was performed at the PTB, the same day as the blackbody calibration. This provided the reference response to be maintained for the next months. We repeated the same measurements in the dark room of the Izaña observatory before the campaign. The ratio of the spectra recorded at the PTB and Izaña represents for each lamp the change of the IRSPERAD response:

$$\mathrm{Corr} = \frac{S_{FEL}(\mathrm{PTB})}{S_{FEL}(\mathrm{IZO})}. \tag{3}$$

The factors $S_{FEL}(\mathrm{PTB})$ and $S_{FEL}(\mathrm{IZO})$ are the composite lamp signal (average of several accumulations) at the PTB and before the campaign at Izaña. Figure 5 shows this correction factor, the raw and filtered data obtained by averaging the composite spectra of the four FEL lamps, along the nominal wavelength sampling (H_2O corrected).

The mean ratio shows a deviation of less than 2 % between 700 nm and 1800 nm. Knowing the time interval between the PTB calibration and the start of campaign (three weeks), the effect of transportation by road and airplane between the PTB, Brussels and Izaña during which the system was disassembled, this uncertainty in the absolute recalibration is acceptable. The concept of the relative calibration using the lamps was fully validated and it preserved the absolute PTB scale of IRSPERAD, within an uncertainty of the correction factor that can be estimated as presented in Section 3.2.2. After the calibration, IRSPERAD was

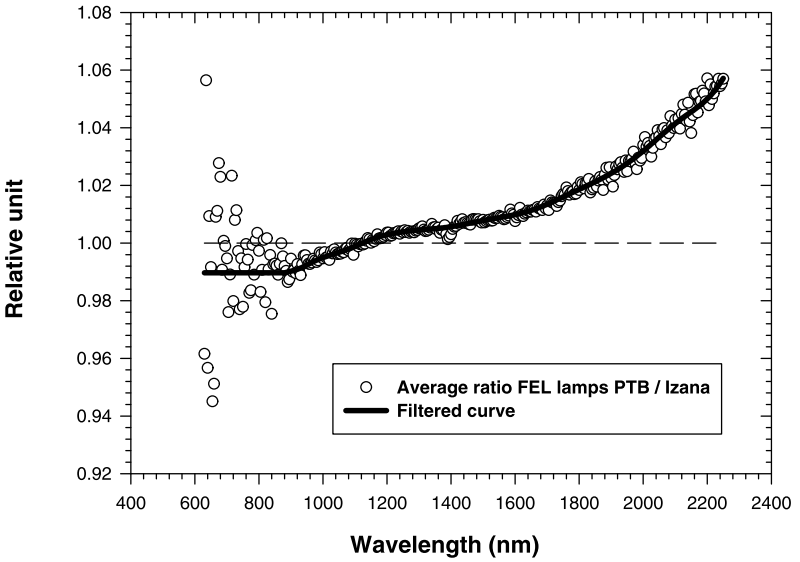

Figure 5 Recalibration of IRSPERAD after the transport from PTB to Izaña, using the four FEL lamps. The points represent the averaged values and the respective filtered curve is also shown.

carefully transported to the outdoor site and repowered immediately. The same relative calibration was performed at the end of the campaign. The ensemble of lamp measurements at PTB permitted the verification and adjustment of their absolute calibration between 600 nm and 2300 nm by the use of the irradiance disseminated by the blackbody, and IRSPERAD. A high coherence was found between the NIST certificate and the recalibration, although a NIST lamp does not present the same geometry as the circular aperture of the blackbody.

2.4. Measurements

2.4.1. Site

The high-mountain Izaña Observatory (IZO), managed by the Izaña Atmospheric Research Centre (IARC), from the State Meteorological Agency of Spain (AEMET) is located in Tenerife (Canary Islands, Spain; at 28.3°N, 16.5°W, 2367 m a.s.l.). A strong temperature inversion layer normally located between 800 m and 1500 m a.s.l., below the Izaña level, prevents the arrival of local or regional pollution from lower levels at the observatory. Consequently, it offers excellent conditions for *in situ* and remote-sensing atmospheric measurements of trace gases and aerosols under free troposphere conditions (Cuevas *et al.*, 2013). This observatory is part of the World Meteorological Organization (WMO) Global Atmospheric Watch Programme (GAW) and part of the Network for the Detection of Atmospheric Composition Change (NDACC). Since 2009 it is part of the Baseline Surface Radiation Network (BSRN; García *et al.*, 2013). Stable total column ozone, very low precipitable water, low aerosol content, and high frequency of clean (> 24 days per month in summertime) and pristine skies (3433 Sun hours/year) make IZO optimal for absolute Sun calibration and validation activities (Puentedura *et al.*, 2012; García *et al.*, 2013). These conditions are only significantly modified by episodic Saharan dust intrusions during summertime (Rodríguez *et al.*, 2009,

2011). IZO is a direct-Sun calibration site of AErosol RObotic NETwork (AERONET; http://aeronet.gsfc.nasa.gov), and is part of the GAW Precision Filter Radiometer (PFR) network, managed by the World Radiation Centre (Davos, Switzerland), and hosts the reference triad of the WMO-GAW Regional Brewer Calibration Centre for Europe (RBCC-E) (http://www.rbcc-e.org).

2.4.2. *Bouguer–Langley Method*

The wavelength-dependent direct transmitted solar irradiance in the atmosphere is described by the Beer–Bouguer–Lambert law, expressed by

$$E(\lambda) = E_0(\lambda) R^{-2} \exp\left[-m(\theta)\tau(\lambda)\right], \tag{4}$$

where E is the irradiance at the top of atmosphere (TOA), m is the air mass factor (AMF) as a function of the solar zenith angle θ, and τ is the optical depth that depends on λ. R^{-2} is the normalization factor to one astronomical unit. Applying the logarithm to Equation (4) leads to

$$\log\left[E(\lambda)\right] = \log\left[E_0(\lambda) R^{-2}\right] - m(\theta)\tau(\lambda). \tag{5}$$

Provided that atmospheric absorption is negligible and $\tau(\lambda)$ remains constant for a series of measurements of $E_0(\lambda)$ taken over a given range of $m(\theta)$ (generally spreading over a half day), the TOA value of $E_0(\lambda)$ is thus the interception on the origin ($m = 0$) of the least-squares fit to the data series $E(\lambda)$ as a function of m. This is a wavelength-dependent law applicable to atmospheric regions where the contributions to optical depth are limited to aerosol and Rayleigh scattering. It is thus not valid in spectral regions of absorption due to atmospheric constituents, namely CO_2, O_2, and H_2O, without a modification as described by Schmid and Wehrli (1995).

2.4.3. *Data Selection*

To identify the spectral regions free of atmospheric absorption, for which the Bouguer–Langley plot method is valid, a method developed by Kindel, Qu, and Goetz (2001) was used after adapting it to our system's bandwidth of 10 nm. The specifics of the IZO measurement site were simulated in the parameters of the model.

This method uses the MODerate resolution TRANsmission (MODTRAN) radiation transfer model to generate a set of ground-based direct Sun irradiance spectra in the wavelength range 0.5 μm $< \lambda <$ 2.5 μm, for AMF values spanning from 1 to 15, by increments of 1. These are used to generate synthetic Langley plots and extrapolate to TOA irradiances. If these replicate the exo-atmospheric SSI input of MODTRAN within 0.7 % and 1.0 % for $\lambda <$ 1.6 μm and $\lambda >$ 1.6 μm, respectively, the associated wavelength is kept for analysis, as illustrated in Figure 6. With this methodology a total of 164 wavelengths were selected and defined as *channels*.

The measurement campaign was carried out between June and October 2011. During this period, approximately 220 Langley plots, corresponding to 220 half-days, have been produced for each of the 164 channels. Spectral irradiance measurements in the custom wavelength sampling range between 600 nm 2310 nm were acquired during the whole day. However, only irradiance measurements acquired for AMF values in the interval 2 to 8 were kept for Langley-plot analysis.

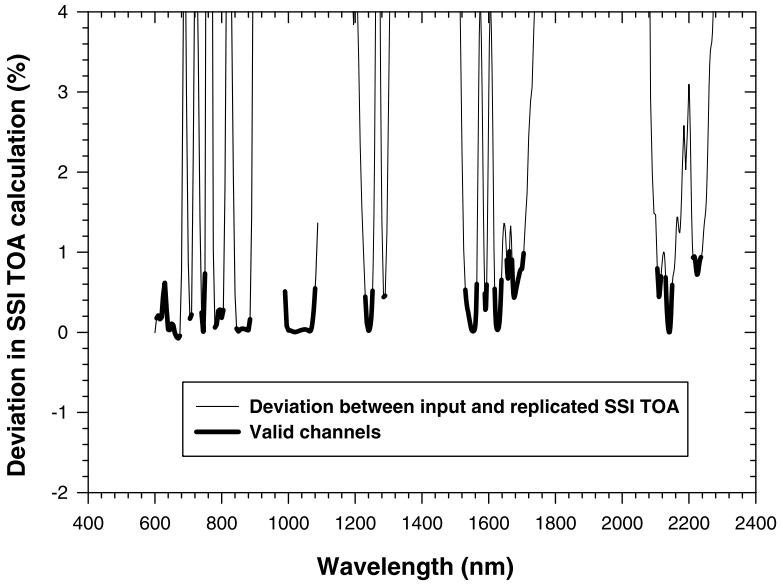

Figure 6 Calculation of the channels that recreated the TOA solar spectrum within 0.7 % to 1.0 %, using Kindel's methodology (see main text).

Data selection process (half-day selection) ensured that the best possible conditions for applying the Langley-plot method were met. Data were screened for the presence of visible clouds using a SONA total-sky camera (Gonzalez, López, and Cuevas, 2012). Enhanced solar irradiance can be generated by multiple scattering of solar light by ice particles present in thin cirrus clouds (Goldfarb *et al.*, 2001; Platt and Dilley, 1984), disturbing the conditions of applications of the Bouguer–Langley law. The presence of invisible cirrus clouds was monitored using corrected backscatter profiles from a Micropulse Lidar (MPL) (Campbell *et al.*, 2002; Hernández *et al.*, 2012). Lidar measurements performed at Santa Cruz de Tenerife, 32 km away from IZO, provided unambiguous information of the possible presence of thin cirrus clouds during measurements.

A second data selection criterion is based on the atmospheric aerosol content during the measurement period. Half days with a low aerosol optical depth (AOD) content and with a variability lower than 10 % were kept for analysis. AOD values were obtained from the AERONET V.2 web database. Figure 7 shows the AOD for the available AERONET wavelengths that overlap our wavelength working range (870 nm, 1020 nm, and 1640 nm) for the first and last days of June 2011. During the first days of June, except for 3 June, the AOD was below 0.02 and 0.008 for both 870 nm and 1020 nm and for 1640 nm, respectively, meaning pristine sky conditions.

A final selection was performed based upon the quality of the Langley plots, keeping only plots with a regression coefficient R^2 of at least 0.99. The application of different data selection steps (cloud screening, aerosol content and stability, and linear regression quality) significantly reduced the number of high-quality Langley plots. From a total of 220 available Langley plots per channel obtained during the whole campaign, 66 were considered as good and kept for further analysis.

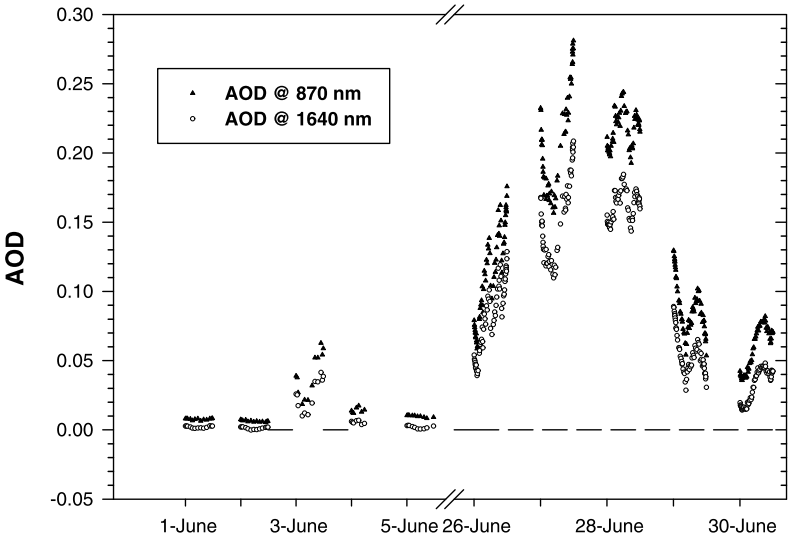

Figure 7 AOD at 870 nm and 1640 nm for the first and the last days of June 2011 is depicted. First days (except 3 June), with quite stable and low AOD (AOD@870 < 0.02, AOD@1640 < 0.005), were suitable to apply the Langley plot method. Higher AOD (AOD@870 $> 0.05 - 0.5$ and AOD@1640 $> 0.015 - 0.020$) and higher AOD variability observed during the last days of the month are due to the presence of Saharan dust over IZO. For the sake of clarity AOD@1020 is not represented because its values are very similar to those of AOD@870.

3. Results

3.1. TOA Solar Irradiance

The irradiance values are obtained with the Langley-plot method using the weighted total least-squares (WTLS) algorithm developed by Krystek and Anton (2007). Irradiance results are grouped into two subsets.

3.1.1. Core Campaign

The first subset corresponds to the first 15 days of campaign. During this period the response loss as well as the change in the wavelength scale of the instrument were considered to be negligible. Nevertheless, fine corrections, due to thermal stress, had to be accounted for in the detector response. These corrections reached a maximum of 1 %.

The uncertainty estimates as described in Section 3.2 are only valid for this subset of data.

Figure 8 shows a high-quality Langley plot obtained on the first day of the campaign. The TOA SSI for the core campaign is shown in Figure 9. Spectral irradiances are averaged over the 18 selected half days of the core campaign.

3.1.2. Whole Campaign

The second subset contains all data from the four-month campaign. The fine corrections mentioned above were still applied but the trend in IRSPERAD absolute response was also

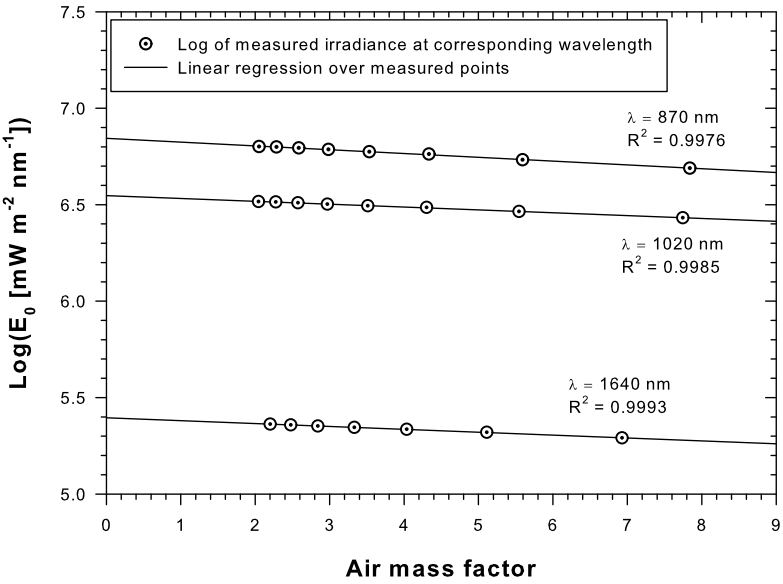

Figure 8 Langley plot for the first half day of the measurement campaign (1 June 2011 AM) for the reference three wavelengths mentioned in Section 2.4.3. The high thermal stability of IRSPERAD and a low and stable aerosol content during the period of measurements (see Figure 7) allowed for high-quality linear regressions ($R^2 > 0.99$).

taken into account. With this purpose, the trend in the absolute response loss was monitored by combining two different methods: a Langley-plot calibration method using the Sun as a relative standard source and a calibration by means of standard FEL lamps. The comparison between the two methods is extensively described in Schmid and Wehrli (1995).

The dataset obtained from Langley-plot method was compared with the one using the ratio of FEL spectra, before and after the campaign. The two methods showed good spectral agreement in the observed trend as a function of wavelength apart from the overall bias of 2.4 % between Sun and FEL reference measurements, as depicted in Figure 10. A spectrally independent shift is more compatible with a geometrical misalignment in the lamp's optical assembly rather than a change in the lamp filament's temperature.

The Sun calibration method was preferred over the lamp method because of the system's mechanical robustness (stability of IRSPERAD on the platform and accurate Sun tracking), the stability of the calibration source (the variability in the NIR is negligible over a period of four months) and the fulfilment of measurement conditions described in Section 2.4.3 (66 half days over a total of 220). The ensemble of these conditions provided a reliable temporal series for studying the instrument response trend during the four-month campaign. This study revealed a well-approximated linear but spectrally dependent trend of the response versus time.

The absolute response was corrected for the loss of response calculation derived from this study. The objective of this relative Sun calibration method was to increase the number of $E_0(\lambda)$ samples to optimize its estimation. Figure 11 shows the Gaussian profile of the distribution of retrieved irradiance values at a given wavelength.

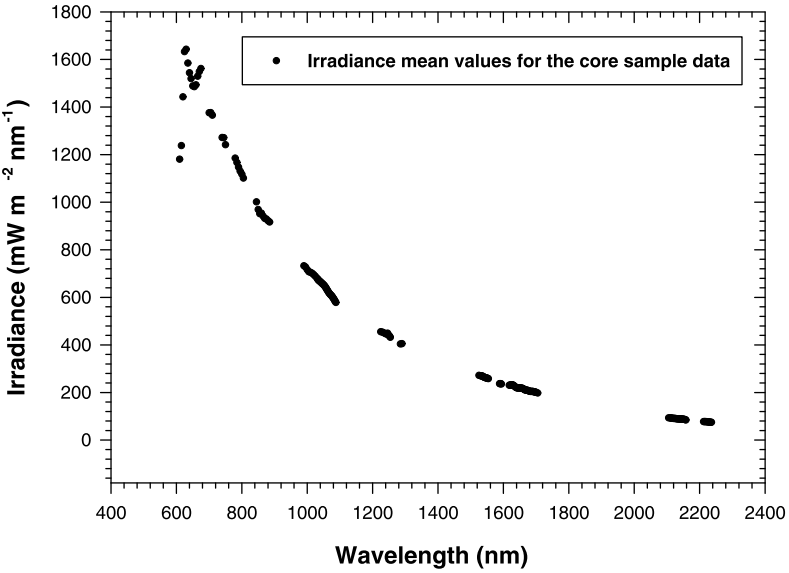

Figure 9 Irradiance values for 164 wavelengths in the NIR atmospheric windows. Each irradiance value was averaged over 16 samples obtained by the Langley-plot method. Each sample corresponds to a selected half day during the core campaign.

Figure 12 shows the relative deviation between the two data subsets. This deviation is lower than 1 % except for the wings of the spectral range. This validates the use of the Sun as the standard source for calibration.

3.2. Uncertainty Calculation

We applied the mathematical formalism of the law of propagation of uncertainties (LPU), according to JCGM (Joint Committee for Guides in Metrology) (2008) to estimate the error on the calculation of TOA SSI values. The study was performed for 11 relevant wavelengths associated with the atmospheric windows. The final TOA SSI, as well as the intermediate uncertainties calculations, are shown in Table 3.

3.2.1. Uncertainties of the PTB Calibration

The absolute response, R, given by Equation (2), was derived from IRSPERAD measurements of the PTB blackbody signal, as described in Section 2.3.1.

The blackbody composite signal, S_{BB}, was obtained by averaging, after dark-current subtraction, several spectral measurements (12 to 22, depending on the spectral range), acquired during a 3 h measurement period. Following LPU, a term C_λ should be added to the definition of S_{BB}. This term describes the eventual signal changes induced by the uncertainty on the instrument's wavelength scale determination (limited to 0.2 nm). However, the contribution of the term C_λ is attenuated and considered to be equal to zero because of the effect of spectral averaging. Furthermore, we assumed that the contribution of electronic noise is included in the standard uncertainty of the blackbody composite signal. The values of $u(S_{\mathrm{BB}})$ are below 1 % for $\lambda > 1$ µm and reach 2 % for 0.8 µm $< \lambda < 1$ µm.

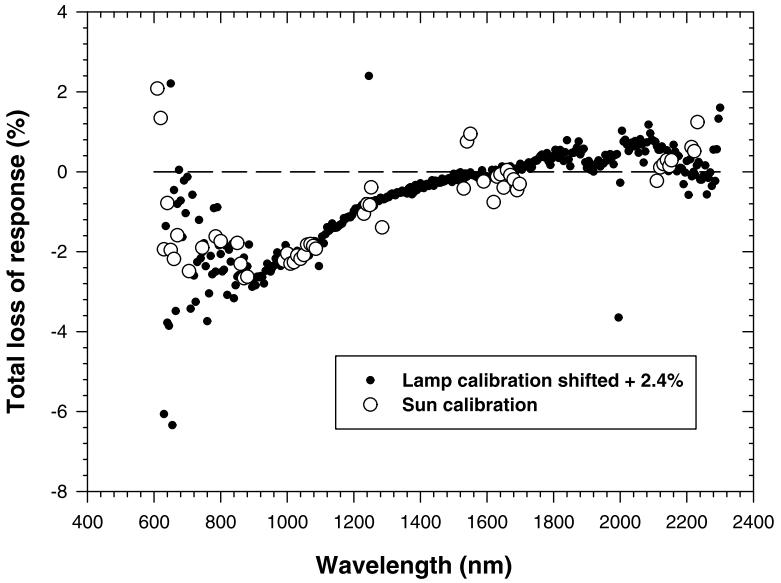

Figure 10 IRSPERAD's loss of response for the duration of the whole campaign, expressed in percentage. These results were obtained by two independent methods using the Sun and the FEL lamps as relative calibration sources, respectively. One can observe the good spectral accordance between the two datasets.

The standard uncertainty, $u(E_{\mathrm{BB}})$, is obtained by deriving the expression for the blackbody spectral irradiance, E_{BB}, given by Equation (1). Knowing the uncertainties on the cavity temperature and its emissivity, on the diameter of the blackbody aperture and on the distance to IRSPERAD, respectively $u(T)$, $u(\epsilon_\lambda)$, $u(D)$, and $u(d)$, we obtained values ranging form 0.13 % to 0.17 % for $u(E_{\mathrm{BB}})$. This demonstrates the high performance of the PTB blackbody as a primary standard of spectral irradiance.

The uncertainty $u(R)$ on the calibration curve is dominated by the contribution of $u(S_{\mathrm{BB}})$. The values of $u(R)$ are lower than 1 % for $\lambda > 1$ µm, dropping to less than 0.5 % for 1 µm $< \lambda <$ 2 µm.

3.2.2. Uncertainties for the Izaña Recalibration

The uncertainty on the recalibration procedure, $u(\mathrm{Corr})$, described previously in Section 2.3.3, is determined by calculating the uncertainty of the correction factor in Equation (3).

The standard uncertainty, $u(S_{\mathrm{FEL}}(*))$, was evaluated for the composite spectrum of each lamp. The contribution of the uncertainties on the lamp distances to IRSPERAD and on angular alignments were limited to 0.5 mm and 2 arcmin, respectively, and were neglected. The terms C_λ that express the uncertainty in the instrument's wavelength scale determination were assigned to zero according to the same reasoning as in Section 3.2.1. Values of $u(S_{\mathrm{FEL}})$ lower than 0.1 % were found for 0.8 µm $< \lambda <$ 1.7 µm. These low values show the benefit of having measurements with long accumulation times and good SNR.

Each of the four FEL lamps presented the same spectral behaviour for the ratio PTB/Izaña shown in Figure 5. Nevertheless, a slight lack of lamp reproducibility of the order of 0.5 % was observed. This was not attributed to IRSPERAD, whose response was proved

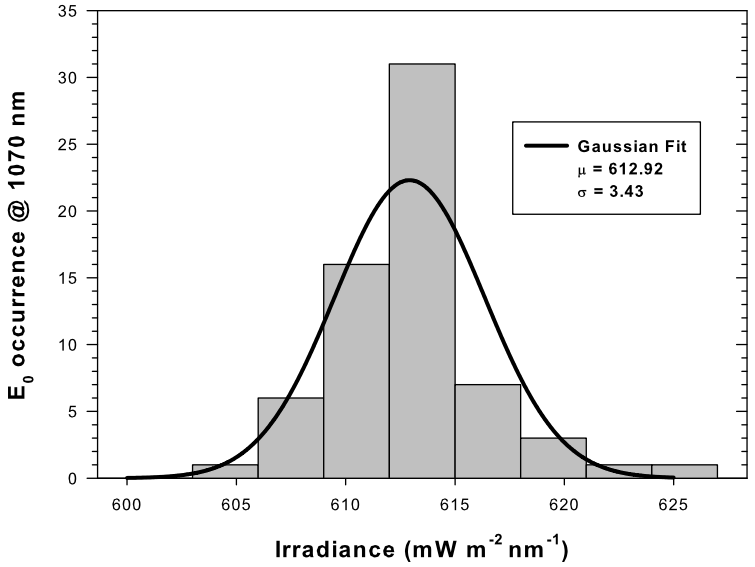

Figure 11 Histogram of the retrieved irradiance at 1070 nm for the 66 half days during the measurement campaign that were kept after applying the selection criteria of measurement conditions. At 1070 nm, the irradiance values distribution has a narrow relative standard deviation of 0.5 %.

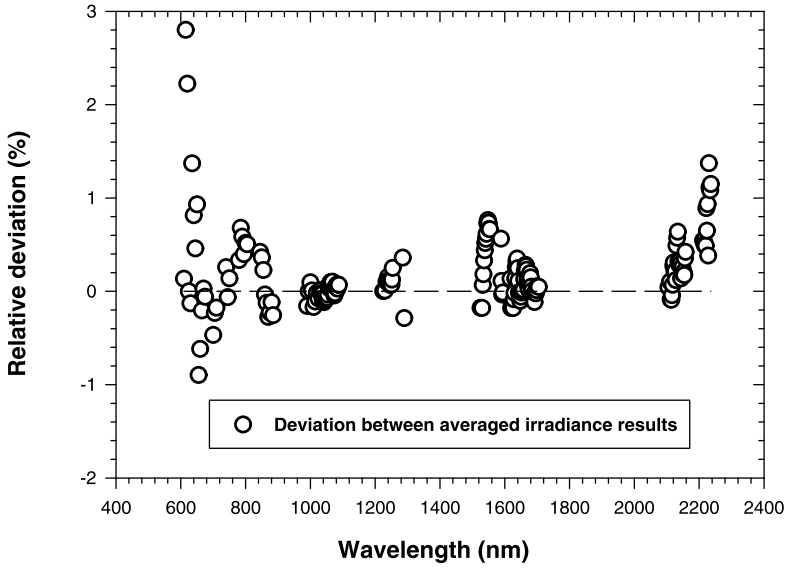

Figure 12 Relative deviations as a function of wavelength between the averaged irradiance values from each data subset (core and whole) as explained in Section 3.1.

to be very stable and reproducible during the many hours of laboratory measurements, but rather to the effect of lamp operations (power supply, stability of the lamp) between power-ups. The uncertainty in the lamp reproducibility was estimated at 0.5 %. This contribution

was integrated into the calculus of $u(\mathrm{Corr})$, for which we obtained values of around 0.6 % for the mid-range wavelengths.

3.2.3. Uncertainties for the Ground-Based Solar Measurements

For IRSPERAD, the spectral irradiance of the Sun for an instantaneous measurement was calculated using the following expression:

$$E = \frac{S_{\mathrm{Iz}} + C_\lambda}{1 - \frac{\alpha_T \Delta T}{100}} R\,\mathrm{Corr}, \tag{6}$$

where S_{Iz} is the electronic output signal obtained for a given solar measurement. R and Corr represent the PTB absolute calibration and the change in response (recalibration) between the PTB and Izaña (in relative units). The parameter α_T is the thermal spectral sensitivity coefficient of IRSPERAD in %/°C. The parameter $\Delta T = T_{\mathrm{PTB}} - T_{\mathrm{Iz}}$ is the difference of temperature between the PTB and the moment that the solar measurement was taken (°C).

The uncertainty calculation was developed only for AMF = 8 for a reference half day, with the purpose of maximizing the uncertainty. Because owing to the low absorption from aerosols and low Rayleigh scattering, the signal recorded for lower AMF values is of the same order of magnitude as that for AMF = 8, which means that the uncertainty calculation is valid for the whole AMF range.

The standard uncertainty due to the noise in the signal was obtained from the SNR study detailed in Section 2.2.1 for the 11 reference wavelengths. Because Sun measurements are instantaneous, the parameter C_λ that represents the uncertainty in the instrument wavelength scale has to be taken into account. For a maximum uncertainty of 0.2 nm in the wavelength calibration, C_λ has a value of 0.2 % at 700 nm and 0.1 % elsewhere, representing the maximum variation in S_{Iz}. Noise and wavelength scale effects were combined by quadratic mean (as independent sources of uncertainty) to provide the final estimate of $u(S_{\mathrm{Iz}})$, and the results show values lower than 1 % except for 700 nm.

For the thermal effects, the uncertainty $u(\Delta T)$ on the temperature (accuracy of 0.1 °C) was considered to be negligible. The uncertainty on the thermal coefficient $u(\alpha_T)$ was estimated from the thermal study, as explained in Section 2.2.3. A constant value of 13.5 % was found between 1 and 1.7 µm for $u(\alpha_T)$ and was extended to the full wavelength range. Although the uncertainty in α_T is significantly high, the low weight of thermal effects on the signal correction (see Table 2) yields a reduced effect in the calculation of $u(E)$.

The standard uncertainty of E was calculated applying LPU to Equation (6). The highly accurate absolute calibration allowed for the SSI to be measured (except for the wings of the spectral range) with an accuracy of 1 % and better, reaching 0.5 % for some wavelengths.

3.2.4. Circumsolar Radiation

The circumsolar radiation is defined as the difference in radiance between the diffuse sky light corresponding to the IRSPERAD field of view (7.16°) and the Sun's angular size ($\approx 0.5°$).

It was computed for one reference day of the campaign, using the Linearized Discrete Ordinate Radiative Transfer Model (LIDORT; Spurr, 2008), for two of the available CIMEL AOD wavelengths (870 and 1020 nm), for AMF values of 8, 5, and 2, and for a surface albedo of 0.3.

The results showed values of circumsolar radiation systematically lower than 0.16 % and 0.10 % at 870 nm and 1020 nm, respectively. This clearly demonstrated the negligible effect

Table 3 Relative standard uncertainties (in %) for the input variables of Equation (6) and its final estimate E for a given instantaneous solar irradiance. The two last columns represent the standard uncertainty for E_0 by two different methods: application of LPU to the Langley plots and the experimental standard deviation of the E_0 sample, as depicted in the example histogram in Figure 11. The calculation was made for 11 reference wavelengths.

λ(nm)	$u(S_{BB})$	$u(E_{BB})$	$u(R)$	$u(S_{FEL})$	u(Corr)	$u(S_{Iz})$	$u(E)$	$u_{LPU}(E_0)$	$u_{distr}(E_0)$
700	8.04	0.17	8.35	3.86+0.5	2.88	2.32	9.13	7.87	1.74
800	2.68	0.16	2.69	0.76+0.5	0.87	0.91	2.97	2.54	1.37
850	1.86	0.16	1.88	0.66+0.5	0.78	0.64	2.14	1.82	1.00
1000	0.46	0.15	0.51	0.14+0.5	0.44	0.22	0.72	0.61	0.59
1070	0.31	0.15	0.34	0.10+0.5	0.42	0.18	0.58	0.49	0.50
1240	0.14	0.14	0.20	0.08+0.5	0.41	0.14	0.49	0.41	0.38
1550	0.18	0.14	0.23	0.09+0.5	0.42	0.16	0.51	0.57	0.35
1620	0.21	0.14	0.36	0.08+0.5	0.41	0.18	0.58	0.65	0.29
1690	0.39	0.14	0.41	0.07+0.5	0.40	0.19	0.62	0.67	0.51
2120	0.68	0.13	0.69	0.15+0.5	0.47	0.42	0.94	1.00	0.79
2200	0.95	0.13	0.97	0.32+0.5	0.61	0.62	1.30	1.37	0.50

of the circumsolar radiation in the NIR under clear-sky conditions at IZO. The conclusion remains valid for $\lambda > 1020$ nm because the atmospheric diffusion decreases with increasing wavelengths.

3.2.5. Uncertainity of the TOA Irradiance

Assuming perfect conditions for the application of the Bouguer–Langley law, we calculated the standard uncertainty on the TOA irradiance, $u(E_0)$ as a function of wavelength with two different methods.

The WLTS method (see Section 3.1) merges the LPU with an ordinary linear regression algorithm knowing the uncertainties in the two coordinates, resulting in the standard uncertainty $u_{LPU}(E_0)$. We assumed no errors in the calculation of the AMF. On the other hand, all systematic and random contributions from the calibration, its transfer, and the conditions of instantaneous solar measurements [see Equation (6)] are enclosed in $u(E)$. The criteria for selecting the 'core' campaign data were strict (see Section 2.4.3) and corresponded to exceptional conditions of application of the Bouguer–Langley law. A possible slight drift of the absolute response (≈ 0.5 %) during the 'core' campaign or some effects due to the residual molecular absorption could also have contributed to additional fluctuations.

The histogram of the distribution of E_0 for a given wavelength follows a Gaussian distribution as depicted in Figure 11. The associated uncertainty, $u_{distr}(E_0)$, is thus the FWHM of a Gaussian curve fit to the histogram. This uncertainty encloses the ensemble of instrumental and atmospheric effects occurring during the full campaign.

The uncertainty values derived from the two methods are shown in the last two columns of Table 3. We found good agreement between them for the central wavelength range. For the wings of the spectral domain, $u_{distr}(E_0)$ showed unexpected lower values.

4. Discussion

We provided new data for the TOA SSI in the NIR, based on a simplified methodology and stable instrumentation (Sun-tracker, spectroradiometer), along with the reliability of the blackbody of the PTB as primary standard source. This allowed us to have full radiometric control over the experimental setup and the error sources. In addition, ideal atmospheric conditions at IZO permitted the optimal application of the Bouguer–Langley method to a large number of measurements. Therefore, we expect that this measurement campaign, supported by careful radiometric investigations and metrology, provides sufficient accuracy of the absolute calibration to provide accurate reference NIR SSI data from the ground.

Recently, some discrepancies were found in the UV and NIR parts of the solar spectrum, measured from instruments in space. In UV, these differences arise from ageing of instruments by UV radiation, caused by photochemical processes as UV polymerization of contaminant deposits on optical surfaces (Floyd *et al.*, 1996), which generates modifications in the instrumental responses. In the NIR, optical components are less sensitive to these effects, but the SNR is generally lower. The comparison between TOA SSI spectra of SCIAMACHY and the ensemble of ATLAS3, SOLAR/SOLSPEC, and IRSPERAD is shown in Figure 13. The deviation between all of the experiments providing TOA SSI in the NIR, described in Section 1, relative to ATLAS3 is shown in Figure 14.

From our ground-based measurements, it is obvious that the discrepancies with respect to ATLAS3 are not compatible with the declared standard uncertainties of the two spectra around the 1.6 μm spectral region (3 % for ATLAS3), as shown in Figures 13 and 14.

The NIR spectra measured by SCHIAMACHY show a similar divergence in amplitude and spectral dependence as SOLAR/SOLSPEC relative to ATLAS3 (Noël *et al.*, 2007), as mentioned in Section 1. The estimated uncertainties are of the order of 2 % for the whole SCIAMACHY wavelength range. For SOLAR/SOLSPEC the uncertainty is lower than 1 % for most of the NIR range, and lower than 2 % for 2.0 μm $< \lambda <$ 2.3 μm (Bolsée, 2012).

The high-altitude measurements of Arvesen, Griffin, and Pearson (1969) agree well with ATLAS3, except for wavelengths around 1.87 μm and above 2.0 μm. The differential found at the region of the wide H_2O absorption band centred at 1.87 μm should have its origin in residuals arising from corrections to the water vapour column transmittance during the calibration. Nevertheless, the use of blackbodies as a primary standard source of spectral irradiance provides more reliable calibrations than those obtained with a 1000 W quartz-halogen lamp. The 3.0 % standard uncertainty of Arvesen, Griffin, and Pearson (1969) is mainly generated by the lamp calibration. Furthermore, the TSI of 1390 Wm^{-2} deduced from their spectrum is known to be too high.

The high-resolution CAVIAR ESS was convoluted to a 10 nm bandwidth, and its deviation from ATLAS3 is shown in Figure 14. The deviation in the range 1.4 μm to 2.4 μm presents the same trend as shown by the SCIAMACHY and SOLAR/SOLSPEC curves and IRSPERAD points. The CAVIAR ESS deviation curve has an uncertainty in the range from 3.3 % to 5.9 %.

The deviation of the SIM spectrum relative to ATLAS3 is indicated in Figure 14. SIM is in accordance with ATLAS3 after the use of a SIM-to-ATLAS3 bias correction (Harder *et al.*, 2010). The correction was applied because the expected uncertainties reached 8 % for SIM above 1.35 μm. The corrected SIM spectrum achieves more plausible TSI and solar brightness temperature values (around 1.6 μm), equivalent to those obtained by ATLAS3. The corrected SIM spectrum is the only one that can be presented in this paper (J. Harder, private communication), although the IRSPERAD results are in accordance within 1.19 % in the broad NIR range between 1 μm and 2.2 μm with respect to the uncorrected SIM spectrum. The SIM-to-ATLAS3 bias correction is indicated on Figure 14 for illustration.

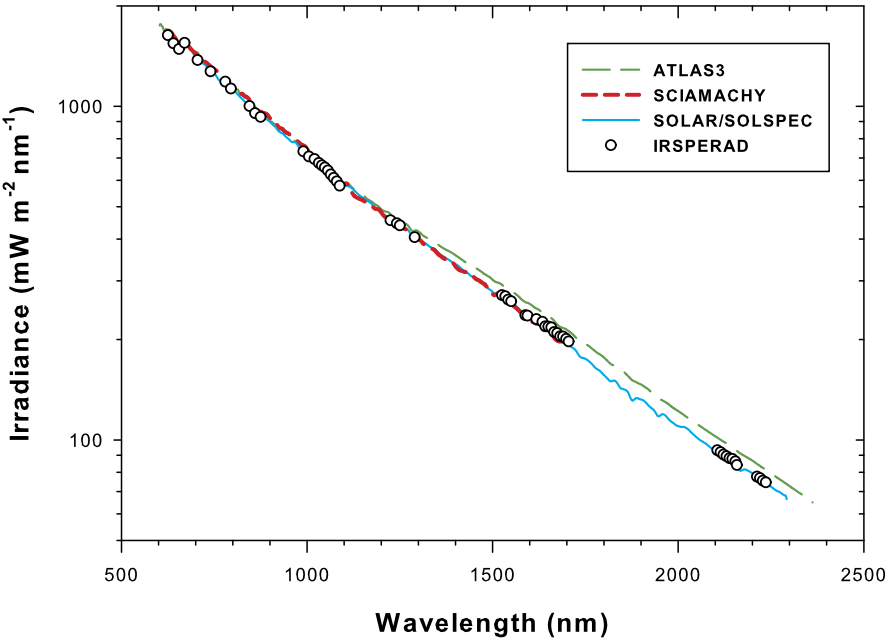

Figure 13 Comparison between different versions of the SOLSPEC instrument (ATLAS3 and SOLAR/SOLSPEC), SCIAMACHY and ground-based measurements performed at Izaña (IRSPERAD). SCIAMACHY, and ATLAS3 are convoluted to 10 nm.

IRSPERAD agrees with recent TOA SSI measurements that show the expected local SSI maximum 1.6 μm that reflects the minimum opacity of the photosphere, but for a lower derived brightness temperature than for ATLAS3. For SOLAR/SOLSPEC, this difference is of about 350 K. Some recent semi-empirical models of the solar photosphere present values 200 K below ATLAS3 (Shapiro *et al.*, 2010; Fontenla *et al.*, 2011).

A meaningful interpretation for the solar physics of measurements providing such a low brightness temperature at 1.6 μm is not the aim of this article. Nevertheless, before new NIR observations can be accepted, it is required that spectroradiometers provide a reliable TSI value (Kopp, Lawrence, and Rottman, 2005) after wavelength integration despite the decrease of spectral irradiance observed in the NIR. Compelling cases can be found, compensating with the visible spectral region for the NIR irradiance deficit. This is the case of SOLAR/SOLSPEC, which provides a TSI of 1357 ± 15 Wm^{-2} after integration (Bolsée, 2012).

The ground-based results we presented here provide some arguments for reconsidering the current choice of the ATLAS3 as the IR reference solar spectrum. We consider that finding a correction factor (systematic error) in our measurement conditions that would reproduce the amplitude and spectral dependence of the differences relative to the ATLAS3 NIR spectrum is no trivial task: The very low optical depth in NIR atmospheric windows and the absence of cirrus clouds allowed us to perform high-quality measurements without inducing large systematic measurement errors. Future actions with the purpose of further validating these measurements might be the following:

– Repeating the measurements with another configuration by leaving the IRSPERAD spectrometer and its container in the dark room while collecting the sunlight from the roof

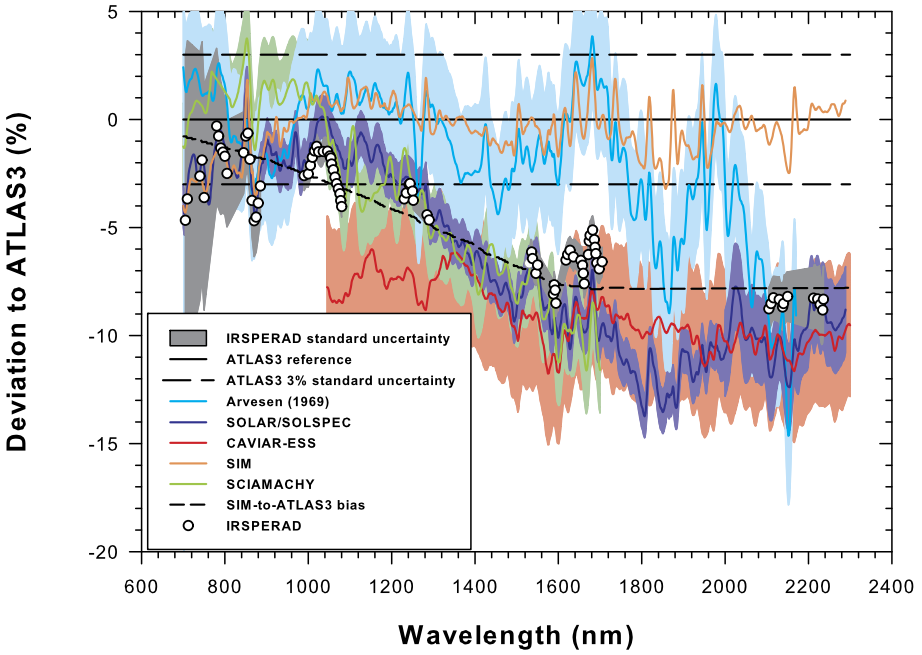

Figure 14 Deviation of TOA SSI between several space and ground-based experiments relative to the reference ATLAS3. All spectra (except SOLAR/SOLSPEC) are convoluted to the IRSPERAD measurements bandwidth of 10 nm. The standard uncertainties of all measurements are depicted. The correction curve between SIM and ATLAS3 is also shown and shows the standard uncertainty of SIM measurements.

with the entrance optic. This configuration could increase the number of relative lamp calibrations without moving the instrument to a concrete platform as we were obliged to, during the campaign.

– Perform a stratospheric balloon flight campaign using the same standard of spectral irradiance for the calibration with adapted instrumentation. The main absorption effects of water vapour would be avoided and the spectral gaps could be filled by widening the atmospheric windows.
– Obviously, the new perspectives that will be offered by the upgraded version of SIM on TSIS will be of great interest for future investigations.

5. Conclusion

We presented the measurement of TOA solar spectral irradiance in the NIR. Using the Bouguer–Langley technique, we found an easy access to this TOA irradiance that complements measurements from space. However, ground-based measurements are limited to a series of NIR wavelengths that correspond to the atmospheric windows. By applying only a few corrections (thermal effects, wavelength-scale trend, and recalibration) and controlling all sources of uncertainties, the TOA irradiance was measured with high accuracy. Important features were the use of the blackbody of the PTB as the primary standard of spectral irradiance, a stable and robust double monochromator from Bentham, and the choice of a quality high-altitude site of measurement, such as IZO. This work was intended to bring

some contributions to the discussion of the solar irradiance around 1.6 μm that corresponds to the minimum opacity value of the solar photosphere.

As for all previous space experiments, we found a good agreement with ATLAS3 for wavelengths up to 1.2 μm. In contrast, in the minimum opacity spectral region up to 2.3 μm we found a discrepancy reaching 6 to 8 % that cannot be explained with the metrology of measurements. In particular, the declared respective standard uncertainties are 3 % for ATLAS3 and only 0.6 to 1.4 % for IRSPERAD in the spectral region we investigated. We noticed that for all recent experiments, either ground-based or from space, the respective spectra show similar deviations with respect to the ATLAS3 spectrum around 1.6 μm, even though they were measured by independent instruments and with different methodologies.

There are therefore open questions arising from recent works in the NIR measurements performed from space by SCHIAMACHY and SOLAR/SOLSPEC as well as from ground-based measurements by CAVIAR ESS and their comparison with ATLAS3. New inputs from the improved version of SIM on TSIS are expected in the near future.

The full IRSPERAD data are available on request or from the online version of this article.

Acknowledgements The authors wish to thank the staff of the Izaña Atmospheric Observatory (IZO, Tenerife) for kindly supporting the campaign, and especially Ramón Ramos, IZO field manager, our colleague Christine Bingen for her thorough reviews of the manuscript, Bruce C. Kindel (University of Colorado, Boulder, USA) for the interest in our work and for kindly providing us the calculations with MODTRAN of the valid Bouguer–Langley channels in the NIR for the 10 nm bandpass of our instrument. M. Weber acknowledges the financial support from the EU SOLID project. The authors acknowledge the support from the Belgian Federal Science Policy Office (BELSPO) through the ESA-PRODEX program and the funding of the Solar-Terrestrial Centre of Excellence (STCE).

References

Arvesen, J.C., Griffin, R.N., Pearson, D.J.: 1969, Determination of extraterrestrial solar spectral irradiance from a research aircraft. *Appl. Opt.* **8**, 2215 – 2232.

Bolsée, D.: 2012, Métrologie de la spectrophotométrie solaire absolue. Principes, mise en oeuvre et résultats. Instrument SOLSPEC à bord de la Station Spatiale Internationale. Ph.D. thesis, Free University of Brussels.

Cahalan, R., Pilewskie, P., Woods, T.: 2012, Free flyer Total and Spectral Solar Irradiance Sensor (TSIS) and climate services mission. EGU General Assembly 2012. *Geophys. Res. Abstr.* **14**, 1886.

Campbell, J., Hlavka, D., Welton, E., Flynn, C., Turner, D., Spinhirnem, J., Scott, V., Hwang, I.: 2002, Full-time, eye-safe cloud and aerosol lidar observation at atmospheric radiation measurement program sites: Instruments and data processing. *J. Atmos. Ocean. Technol.* **19**, 431 – 442.

CIMO (Comission for Instruments and Methods of Observation): 2008, *CIMO: Guide to Meteorological Instruments and Methods of Observation*, WMO, Geneve, I.7-5.

Cuevas, E., González, Y., Rodríguez, S., Guerra, J.C., Gómez-Peláez, A.J., Alonso-Pérez, S., Bustos, J., Milford, C.: 2013, Assessment of atmospheric processes driving ozone variations in the subtropical North Atlantic free troposphere. *Atmos. Chem. Phys.* **13**, 1973 – 1998.

Floyd, L.E., Herring, L.C., Prinz, D.K., Brueckner, G.E.: 1996, Maintaining calibration during the long-term space flight of the Solar Ultraviolet Spectral Irradiance Monitor (SUSIM). In: Huffman, R.E., Stergis, C.G. (eds.) *Ultraviolet Atmospheric and Space Remote Sensing: Methods and Instrumentation*, *Proc. SPIE* **23**, 36 – 47.

Fontenla, J.M., Harder, J.W., Rottman, G., Woods, T.N., Lawrence, G.M., Davis, S.: 2004, The signature of solar activity in the infrared spectral irradiance. *Astrophys. J. Lett.* **605**, L85 – L88.

Fontenla, J.M., Avrett, E., Thuillier, G., Harder, J.: 2006, Semiempirical models of the solar atmosphere. I. The quiet and-active Sun photosphere at moderate resolution. *Astrophys. J.* **639**, 441 – 458.

Fontenla, J.M., Harder, J., Livingston, W., Snow, M., Woods, T.: 2011, High-resolution solar spectral irradiance from extreme ultraviolet to far infrared. *J. Geophys. Res.* **116**, D20108.

Friedrich, R., Fischer, J., Strock, M.: 1995, Accurate calibration of filter radiometers against a cryogenic radiometer using a trap detector. *Metrologia* **32**, 509 – 513.

García, R.D., García, O.E., Cuevas, E., Cachorro, V.E., Romero-Campos, P.M., Ramos, R., Frutos, A.M.: 2013, Solar irradiance measurements compared to simulations at the BSRN Izaña station. Mineral dust radiative forcing and efficiency study. *J. Geophys. Res.* DOI.

Goldfarb, L., Keckhut, P., Chanin, M.L., Hauchecorne, A.: 2001, Cirrus climatological results from Lidar measurements at OHP. *Geophys. Res. Lett.* **28**, 1687 – 1690.

Gonzalez, Y., López, C., Cuevas, E.: 2012, Automatic observation of cloudiness: Analysis of all-sky images. In: *WMO Technical Conference on Meteorological and Environmental Instruments and Methods of Observation. Session 3*. http://www.wmo.int/pages/prog/www/IMOP/publications/IOM-109_TECO-2012/Session3/O3_01_Gonzales_Automatic_obs_cloudiness.pdf.

Harder, J.W., Thuillier, G., Richard, E.C., Brown, S.W., Lykke, K.R., Snow, M., McClintock, W.E., Fontenla, J.M., Woods, T.N., Pilewskie, P.: 2010, The SORCE SIM solar spectrum: Comparison with recent observations. *Solar Phys.* **263**, 3 – 24.

Harder, J., Lawrence, G., Rottman, G.J., Woods, T.N.: 2000, The Spectral Irradiance Monitor (SIM) for the SORCE mission. In: Barnes, W.L. (ed.) *Earth Observing Systems V.*, *Proc. SPIE* **4135**, 204 – 214.

Harder, J., Lawrence, G.M., Fontenla, J.M., Rottman, G., Woods, T.N.: 2005, The spectral irradiance monitor: Scientific requirements, instrument design, and operation modes. *Solar Phys.* **230**, 141 – 167.

Hernández, Y., Alonso-Pérez, S., Cuevas, E., de Bustos, J., Gomez-Peláez, A., Ramos, R., Córdoba-Jabonero, C., Gil, M.: 2012, Planetary boundary layer and Saharan air layer top height determination using ceilometer and micro pulse lidar intercomparison for two case studies. 2012 European Aerosol Conference, Abstract A-WG02S1P51. http://www.eac2012.com/EAC2012Book/files/1035.pdf.

JCGM (Joint Committee for Guides in Metrology): 2008, *Evaluation of Measurement Data – Guide to the Expression of Uncertainty in Measurement*, BIPM, Paris, 21 – 22.

Kindel, B.C., Qu, Z., Goetz, A.F.H.: 2001, Direct solar spectral irradiance and transmittance measurements from 350 to 2500 nm. *Appl. Opt.* **40**, 3483 – 3494.

Kopp, G., Lawrence, G., Rottman, G.: 2005, The Total Irradiance Monitor (TIM): Science results. *Solar Phys.* **230**, 129 – 140.

Kruse, P.W., McGlauchlin, L.D., McQuistan, R.B.: 1962, *Elements of Infrared Technology. Generation, Transmission and Detection*, Wiley, New York, 265 – 268.

Krystek, M., Anton, M.: 2007, A weighted total least-squares algorithm for fitting a straight line. *Meas. Sci. Technol.* **18**, 3438 – 3442.

Mandel, H., Labs, D., Thuillier, G., Hersé, M., Simon, P.C., Gillotay, D.: 1998, Calibration of the SOLSPEC spectrometer to measure the irradiance from space. *Metrologia* **35**, 697 – 700.

Menang, K.P., Ptashnik, I.V., Coleman, M.D., Gardiner, T.D., Shine, K.P.: 2013, A high-resolution near-infrared extraterrestrial solar spectrum derived from ground-based Fourier transform spectrometer measurements. *J. Geophys. Res.* **118**, 1 – 13.

Mohr, P.J., Taylor, B.N.: 2005, CODATA recommended values of the fundamental physical constants: 2002. *Rev. Mod. Phys.* **77**, 1 – 107.

Neckel, H., Labs, D.: 1984, The solar spectrum between 3300 and 12500 Å. *Solar Phys.* **90**, 205 – 258.

Noël, S., Bovensmann, H., Burrows, J.P., Frerick, J., Chance, K.V., Goede, A.P., Muller, C.: 1998, SCIAMACHY instrument on ENVISAT-1. In: Fujisada, H. (ed.) *Sensors, Systems, and Next-Generation Satellites II*, *Proc. SPIE* **3498**, 94 – 104.

Noël, S., Kokhanovsky, A.A., Jourdan, O., Gerilowski, K., Pfeilsticker, K., Weber, M., Bovensmann, H., Burrows, J.P.: 2007, SCIAMACHY reflectance and solar irradiance validation. In: Danesy, D. (ed.) *Proc. Third Workshop on the Atmospheric Chemistry Validation of ENVISAT (ACVE-3)*, *ESA SP-642*, on CDROM.

Pagaran, J., Weber, M., Burrows, J.P.: 2009, Solar variability from 240 to 1750 nm in terms of faculae brightening and sunspot darkening from SCIAMACHY. *Astrophys. J.* **700**, 1884 – 1895.

Pagaran, J., Harder, J.W., Weber, M., Floyd, L.E., Burrows, J.P.: 2011, Intercomparaison of SCIAMACHY and SIM vis-IR irradiance over several solar rotational timescales. *Astron. Astrophys.* **528**, A67.

Platt, C.M.R., Dilley, A.C.: 1984, Determination of the cirrus particle single scattering phase function from lidar and solar radiometric data. *Appl. Opt.* **23**, 380 – 386.

Puentedura, O., Gil, M., Saiz-Lopez, A., Hay, T., Navarro-Comas, M., Gomez-Pelaez, A., Cuevas, E., Iglesias, J., Gomez, L.: 2012, Iodine monoxide in the north subtropical free troposphere. *Atmos. Chem. Phys.* **12**, 4909 – 4921.

Rodríguez, S., González, Y., Cuevas, E., Ramos, R., Romero, P.M., Abreu-Afonso, J., Redondas, A.: 2009, Atmospheric nanoparticle observations in the low free troposphere during upward orographic flows at Izaña Mountain Observatory. *Atmos. Chem. Phys. Discuss.* **9**, 10913 – 10956.

Rodríguez, S., Alastuey, A., Alonso-Pérez, S., Querol, X., Cuevas, E., Abreu-Afonso, J., Viana, M., Pérez, N., Pandolfi, M., de la Rosa, J.: 2011, Transport of desert dust mixed with North African industrial pollutants in the subtropical Saharan Air Layer. *Atmos. Chem. Phys.* **11**, 6663 – 6685.

Sapritsky, V.I., Khlevnoy, B.B., Khromchenko, V.B., Lisiansky, B.E., Mekhontsev, S.N., Melenevsky, U.A., Morozova, S.P., Prokhorov, A.V., Samoilov, L.N., Shapoval, V.I., Sudarev, K.A., Zelener, M.F.: 1997, Precision blackbody sources for radiometric standards. *Appl. Opt.* **36**, 5403 – 5408.

Schmid, B., Wehrli, C.: 1995, Comparison of Sun photometer calibration by use of the Langley technique and the standard lamp. *Appl. Opt.* **34**, 4500 – 4512.

Shapiro, A., Schmutz, W., Schoell, M., Haberreiter, M., Rozanov, E.: 2010, NLTE solar irradiance modeling with the COSI code. *Astron. Astrophys.* **517**, A48.

Sperfeld, P., Pape, S., Barton, B.: 2010, From primary standard to mobile measurements. Overview of the spectral irradiance calibration equipment at PTB. *Mapan* **25**, 11 – 19.

Sperfeld, P., Raatz, K.H., Nawo, B., Müller, W., Metzdorf, J.: 1995, Spectral-irradiance scale based on radiometric black-body temperature measurements. *Metrologia* **32**, 435 – 439.

Sperfeld, P., Metzdorf, J., Galal Yousef, S., Stock, K.D., Müller, W.: 1998a, Improvement and extension of the black-body-based spectral irradiance scale. *Metrologia* **35**, 267 – 271.

Sperfeld, P., Galal Yousef, S., Metzdorf, J., Nawo, B., Müller, W.: 2000, The use of self-consistent calibrations to recover absorption bands in the black-body spectrum. *Metrologia* **37**, 373 – 376.

Spurr, R.: 2008, LIDORT and VLIDORT: Linearized pseudo-spherical scalar and vector discrete ordinate radiative transfer models for use in remote sensing retrieval problems. In: Kokhanovsly, A. (ed.) *Light Scattering Reviews* **3**, Springer, Berlin, 229 – 271.

Taubert, D.R., Friedrich, R., Hartmann, J., Hollandt, J.: 2003, Improved calibration of the spectral responsivity of interference filter radiometers in the visible and near infrared spectral range at PTB. *Metrologia* **40**, S35 – S38.

Thuillier, G., Simon, P.C., Labs, D., Pastiels, R., Neckel, H.: 1981, An instrument to measure the solar spectrum from 170 to 3200 nm on board Spacelab. *Solar Phys.* **74**, 531 – 537.

Thuillier, G., Hersé, M., Labs, D., Foujols, T., Peetermans, W., Gillotay, D., Simon, P.C., Mandel, H.: 2003, The solar spectral irradiance from 200 to 2400 nm as measured by the SOLSPEC spectrometer from the ATLAS and EURECA missions. *Solar Phys.* **214**, 1 – 22.

Thuillier, G., Foujols, T., Bolsée, D., Gillotay, D., Hersé, M., Peetermans, W., Decuyper, W., Mandel, H., Sperfeld, P., Pape, S., Taubert, D.R., Hartmann, J.: 2009, SOLAR/SOLSPEC: Scientific objectives, instrument performance and its absolute calibration using a blackbody as primary standard source. *Solar Phys.* **257**, 185 – 213.

Thuillier, G., Bolsée, D., Schmidtke, G., Foujols, T., Nikutowski, B., Shapiro, A., Schmutz, W., Brunner, R., Erhardt, C., Hersé, M., Gillotay, D., Petermanns, W., Decuyper, W., Pereira, N., Mandel, H.: 2013, The solar irradiance spectrum at solar activity minimum between solar cycles 23 and 24. *Solar Phys.* DOI.

Werner, L., Fischer, J., Johannsen, U., Hartmann, J.: 2000, Accurate determination of the spectral responsivity of silicon trap detectors between 238 and 1015 nm. *Metrologia* **37**, 279 – 284.